



UNIVERSITEIT•STELLENBOSCH•UNIVERSITY
jou kennisvenoot • your knowledge partner

Design and Evaluation of a Magnetically Geared PM Machine
(repository copy)

Article:

Gerber, S. and Wang, R-J., (2015) Design and Evaluation of a Magnetically Geared PM Machine, *IEEE Transactions on Magnetics*, 51(8): 8107010, Aug. 2015; ISSN: 1941-0069

<https://doi.org/10.1109/TMAG.2015.2421474>

Reuse

Unless indicated otherwise, full text items are protected by copyright with all rights reserved. Archived content may only be used for academic research.

Design and Evaluation of a Magnetically Geared PM Machine

Stiaan Gerber¹, Rong-Jie Wang¹

¹Department of Electrical and Electronic Engineering, Stellenbosch University, Stellenbosch, South Africa

This paper presents the design and evaluation of a magnetically geared permanent magnet machine with an inner stator. A brief overview of relevant operating principles is first given. A simplified design and simulation methodology which can ensure that the magnetic gear and the stator are well matched, is then devised. The method is applied to the design optimization of a small machine resulting in a design with a maximum torque density of 115 kNm/m^3 per active volume. To validate the design, a working prototype has been built and experimentally evaluated. It shows that this computationally efficient design methodology is well suited for the optimization of magnetically geared permanent magnet machines. Finally, a method of analyzing the operating points of the machine is described. Relevant conclusions are drawn and recommendations for future work are given.

Index Terms—Special electrical machines, magnetic gears, permanent magnet machines, finite element method, design optimization

I. INTRODUCTION

MAGNETICALLY geared machines (MGMs) are a new class of electrical machine that integrate a conventional permanent magnet machine with a magnetic gear. These machines are worth considering because of the exceptionally high torque density that they offer compared to conventional electrical machines. Compared to mechanically geared systems, MGMs promise to be low maintenance devices with no frictional wear and a long service life. Potential applications include wind power generation [1], traction motors [2], ship propulsion and many industrial applications.

Magnetically geared machines with various topologies can be realized. To date, the configurations that have received the greatest interest are machines with a stator fitted inside a magnetic gear, as shown in Fig. 1(a) [2] [3] [4], and machines with a stator replacing the outer back yoke of a magnetic gear, as shown in Fig. 1(b) [5] [6]. Axial flux configurations can also be realized [7]. In general, magnetically geared machines can be classified as either magnetically coupled or decoupled machines, depending on whether the electrical machine and magnetic gear components share common flux paths or not. The topology in Fig. 1(a) can be realized as either a coupled configuration, as illustrated in the figure, or as a decoupled configuration [8]. The topology in Fig. 1(b) can be classified as a coupled configuration.

In this paper, the focus falls on the design and evaluation of a coupled MGM with an inner stator. A special structure is proposed for the high-speed rotor which minimizes the space required for this component while reducing losses and allowing a high torque density to be achieved. Section II gives a brief overview of relevant theory. The analysis and optimization methods employed are discussed in sections III and IV. Thereafter, the fabrication and experimental evaluation of the prototype is presented in sections V and VI. Finally, conclusions are drawn and key areas for future work are identified.

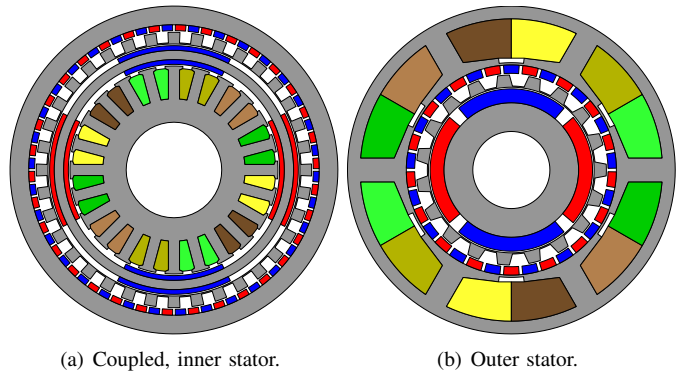


Fig. 1. Two popular topologies of magnetically geared machines.

II. NOMENCLATURE AND BASIC THEORY

The nomenclature used when describing magnetic gears and magnetically geared machines is not well established. Some descriptions can be ambiguous. For clarity's sake, this section describes the conventions used in this paper and briefly reviews relevant concepts.

The term magnetic gear is used to refer to a gear such as described in [9] and illustrated in Fig. 2. Other types of magnetic gears exist such as planetary gears [10], cycloidal gears [11] [12] and harmonic gears [13]. The type of gear in Fig. 2 is especially suited to integration with electrical machines because of its simple concentric structure. This type of gear can be described as a flux-modulated magnetic gear. It consists of three components, which perform functions analogous to the components of mechanical planetary gears. The inner and outer assemblies are simply gears with teeth replaced by magnets. For this reason, these components are named according to their mechanical planetary counterparts, as illustrated in Fig. 2. In flux-modulated magnetic gears, the modulator performs the function of the planet gear assembly in a planetary gear. This component facilitates the magnetic coupling between the sun and the ring gears. The relationship between the number of pole-pairs on the sun and ring gears

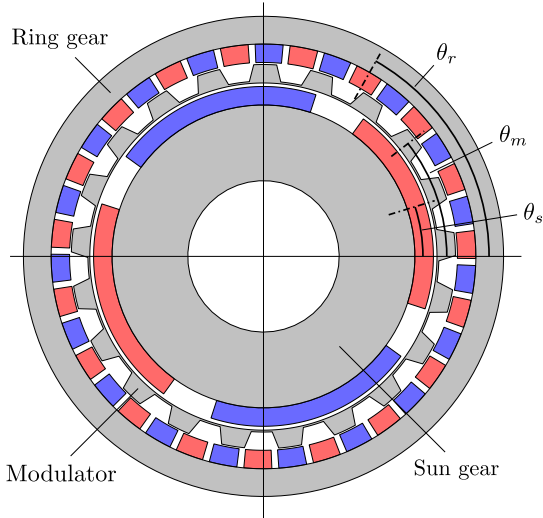


Fig. 2. A flux-modulated magnetic gear.

and the number of modulator segments is

$$q_m = p_s + p_r \quad (1)$$

with q_m the number of modulator segments, p_s the number of pole-pairs on the sun gear and p_r the number of pole-pairs on the ring gear. The torque on the components increase sinusoidally with the load angle of the magnetic gear, δ_g which is defined as (see appendix for a derivation)

$$\delta_g = p_s \theta_s + p_r \theta_r - q_m \theta_m \quad (2)$$

with the angles θ_s , θ_r and θ_m defining the angular positions of the components relative to an arbitrary reference, as shown in Fig. 2. The torque on the modulator, for example, can be described as

$$T_m = T'_m \sin \delta_g \quad (3)$$

where T'_m is called the pull out torque or stall torque and is the maximum torque that can be transferred by the modulator. If this torque is exceeded, the gear will slip.

During steady-state operation, the load angle is constant and a relationship between the rotational speeds of the components can be obtained by taking the derivative of (2):

$$p_s \omega_s + p_r \omega_r - q_m \omega_m = 0 \quad (4)$$

Just like planetary gears, flux-modulated magnetic gears can operate in different modes, depending on which component's movement is constrained. Throughout this paper, the mode of operation with a grounded ring gear ($\omega_r = 0$) is considered. In this case, the modulator is coupled to the low-speed machine shaft. The resulting gear ratio between the sun gear and the modulator is:

$$G_r = \frac{q_m}{p_s} \quad \omega_s = G_r \omega_m \quad T_m = -G_r T_s \quad (5)$$

A magnetically geared machine is an electrical machine that essentially contains a complete magnetic gear as part of an integrated entity. It can be viewed as a magnetic gear with an additional component, the stator. The stator is equipped with a p_s pole-pair winding, and thus its field interacts directly

with that of the sun gear. As mentioned in the introduction, several topologies exist. In magnetically geared machines, the following relationship holds:

$$T_i + T_s + T_m + T_r = 0 \quad (6)$$

where T_i is the torque exerted on the stator (the subscript i refers to the source of the magnetic field: the winding current). The other terms refer to the total torque on the sun gear, modulator and ring gear respectively. If the terms for the stator torque and sun gear torque are grouped such that $T_{is} = T_i + T_s$, the modulator torque can be expressed as

$$T_m = -G_r T_{is} \quad (7)$$

$$= -G_r (T_i + T_s) \quad (8)$$

Thus, in an MGM, the reaction torque generated by the modulator is split between the sun gear and the stator. The above equation shows that an MGM can also be operated as a power splitting device. For example, if torque is applied to the modulator, a portion of the input power can be diverted to a high-speed output shaft connected to the sun gear and the remainder can be converted to electrical power. This paper, however, is concerned with the design of an MGM which is to operate purely as an electrical machine. This implies that, in steady-state operation, the net torque on the sun gear should be zero.

III. DESIGN ANALYSIS METHODOLOGY

In this section, an efficient approach to designing magnetically geared machines is devised which employs 2D static finite element simulations to limit the computational cost.

A. Matching of the magnetic gear and the stator

The design of an MGM entails the design of two different torque transfer mechanisms, the magnetic gear and the electrical machine. In order to ensure that the stator and magnetic gear components of a magnetically geared machine are well matched, they must both be rated for the same operating point where the net torque on the sun gear is zero, as explained in the previous section. The balance between these components for the machine in Fig. 1(b) has been investigated in [14].

With regards to component matching, it is useful to define the stator load factor of the machine as follows:

$$\gamma_i = -\frac{G_r T'_i}{T'_m} \quad (9)$$

where G_r is the gear ratio of the machine. T'_i is the rated stator torque and T'_m is the stall torque of the modulator. The minus sign is required to make the factor positive, since T'_i and T'_m have opposite signs. The stator load factor is a measure of the balance between the maximum torque capability of the magnetic gear and the electrical machine components of an MGM. When $\gamma_i = 1$, the machine is rated to operate at the stall torque of the gear. For a well balanced design, the stator load factor should generally be less than one seeing as operating too close to the stall torque of the gear can lead to instability (slipping). Note that in coupled MGMs, the

modulator stall torque T'_m is also influenced by the stator field, although the impact of the stator field is usually small.

The stator load factor can be used to assess the balance of the components in the machine without having to find an operating point satisfying $T_s = 0$. The rated torque of the machine can be determined and appropriate sizing of the stator can be ensured. This approach is applicable to MGMs with both inner and outer stator topologies.

B. Single point simulation

Although, the relationship between the different torque components in a coupled MGM is complex, the design of these machines using the finite element method can be simplified if the following strategy is employed:

- Assume that the stator field does not have a significant impact on the modulator stall torque
- Simulate the point with $\delta_g = 90^\circ$, $\alpha = 90^\circ$ and rated current, where α is the current angle relative to the sun gear d-axis.

These assumptions allow the machine to be characterized using a single point finite element analysis. The simulated modulator torque is T'_m and the stator torque is T'_i , which allows the stator load factor to be calculated using (9). Because the torque on the various components due to the magnetic gear is usually very smooth, the average value can be estimated accurately from a single point. This is not the case for the torque produced by the stator because significant cogging torque can be present. For this reason, the torque on the stator is calculated as

$$\bar{T}_i = \frac{3}{2} p_s (\lambda_d i_q - \lambda_q i_d) \quad (10)$$

where λ_d , λ_q are the dq flux linkages and i_d , i_q are the dq currents. This formula gives a good estimate of the average stator torque. When calculating the stator torque in this way, the torque on the sun gear should be obtained as follows:

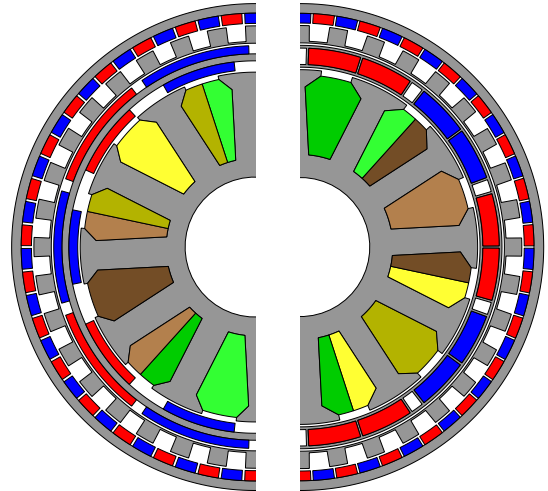
$$\bar{T}_s = -\frac{T_m}{G_r} - \bar{T}_i \quad (11)$$

In this way, the effect of the stator torque ripple on the sun gear can be eliminated while satisfying (6).

C. Loss calculations

Accurate loss calculations are difficult to obtain using a single point simulation. A rough estimate of the core loss can be obtained by extracting flux densities in representative parts of the machine and then calculating the loss using a Steinmetz approach. The calculation of the eddy current losses in the magnets is also challenging. Analytical methods are sensitive to model parameters. Numerical methods are computationally expensive.

In this work, the analysis was performed considering only copper loss, which was expected to account for the majority of the losses at rated conditions. Several factors limit the other loss components. A relatively low frequency was chosen to limit the core and magnet losses. The sun gear magnets are largely shielded from harmful harmonics, whereas the ring gear magnets, though exposed, have a small pitch which serves to limit the eddy currents.



(a) Yoke with surface mounted magnets on both sides.

(b) Laminated carrier securing magnets in cavities.

Fig. 3. Cross section of two coupled magnetically geared machines with different sun gear configurations.

IV. DESIGN OPTIMIZATION

The design optimization of a small magnetically geared machine was performed using the aforementioned analysis strategy, as first reported in [8]. From literature, it is clear that end-effects that are neglected in 2D finite element analysis (FEA) can have a significant detrimental effect on the performance of magnetically geared machines [3], [15]. However, it has been shown in [15] that the optimum values for design parameters exhibit the same tendency in 2D and 3D FEA. Here, the approach has been to optimize using 2D FEA and to calculate the performance of the final design accurately using 3D FEA.

Three variations of the MGM topology with an inner stator were investigated, including coupled and decoupled machines. In [8], it was found that the coupled topology could achieve higher torque ratings within the design constraints. In this paper, a comparison is made between two coupled machines. The one features a surface mounted configuration for the sun gear and the other employs a special laminated carrier ring into which magnets are inserted. These two machines are depicted in Fig. 3. The geometric design variables used in the optimizations are illustrated in Fig. 4 [8].

The design constraints for the prototype are listed in Table I [8]. The diameter and stack length were chosen to facilitate simple construction and to limit the cost of prototyping. The air-gap length is a critical parameter. It has a great impact on the torque capability and the usage of magnet material. The value was chosen as a compromise between performance and manufacturability. The current density was limited so that the machine can be naturally cooled. The winding fill factor was chosen as an estimate of the value that could be achieved with the applicable manufacturing process.

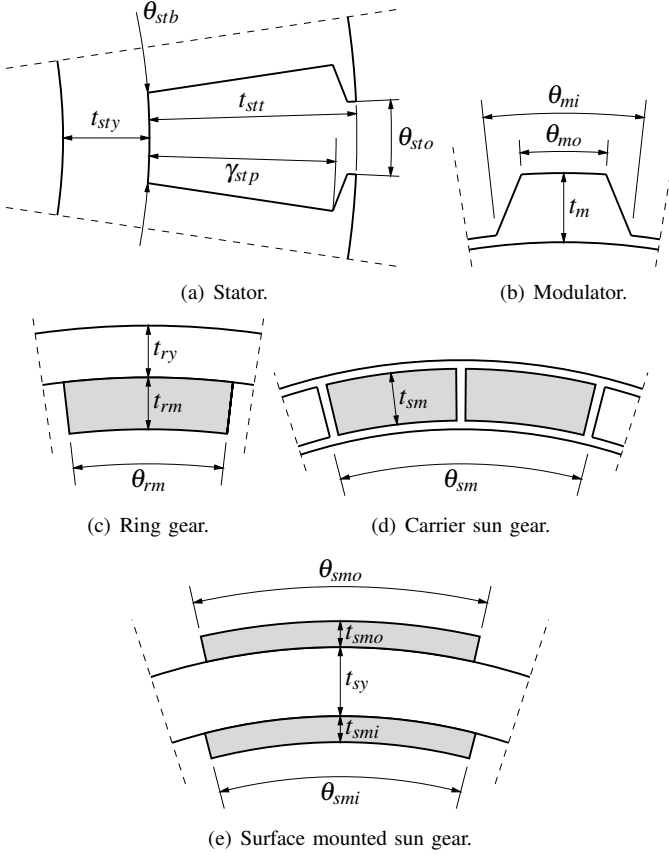


Fig. 4. Design variables for various components of the magnetically geared PM machine.

TABLE I
MACHINE SPECIFICATIONS

Parameter	Value
Outer diameter	140 mm
Stack length	50 mm
Air-gap length	0.7 mm
Maximum current density	5 A/mm ²
Winding fill factor	0.55

The optimization problem was formulated as

$$\text{Maximize: } F(\mathbf{X}) = T'_m/M \quad (12)$$

$$\text{Subject to: } \gamma_i > 0.8 \quad (13)$$

M is the active mass of the machine. The constraint states that the stator load factor should be greater than 0.8. The selected limit of 0.8 implies that the machine will be rated to operate at 80% of the magnetic gear's stall torque, thus leaving a 20% margin. Note that a successful optimization will drive the design to this constraint boundary. This can be understood considering that if a design does not lie on this constraint boundary, it will always be possible to achieve a better design in terms of the objective function which still satisfies the constraint. Thus, a design which does not lie on this constraint boundary, can not be optimal.

Additional measures were taken to protect the magnets from possible demagnetization. For the topology with the magnet

TABLE II
COMPARISON BETWEEN DIFFERENT SUN GEAR TOPOLOGIES

Parameter	Magnet carrier	Surface mounted magnets
Sun gear magnet loss	2.45 W	26.91 W
Sun gear core loss*	3.14 W	1.28 W
Total loss	103.9 W	126.4 W
Stall torque	88.2 Nm	94.4 Nm

* Assuming a laminated carrier and a laminated yoke in the surface mounted configuration.

carrier, a constraint was added which states that the thickness of the ring gear magnets t_{rm} should be at least 60% of the thickness of the sun gear magnets. The 60% ratio was found to give good results. An alternative approach would be to include a demagnetization analysis in the optimization. In that case, it may be necessary to simulate additional operating points since the single point described in the previous section is not necessarily the critical point from a demagnetization perspective. The optimum designs of both machines were evaluated for demagnetization using 3D FEA.

A gradient-based algorithm, the modified method of feasible directions (MMFD) [16], was employed to solve the optimization problems.

Table II lists a few important differences between the two optimum designs. The losses were calculated using transient 2D FEA, with the machine operating at rated current and 200 rpm (modulator speed), corresponding to an operating frequency of 120 Hz. The eddy current loss generated in the sun gear magnets is significantly higher in the surface mounted case. Note that the stator winding generates a strong sub-harmonic which contributes to these losses, along with slotting effects. The majority of the losses occur in the inner magnets (stator side) of the surface mounted configuration. The magnet carrier effectively shields the sun gear magnets from harmful flux pulsations. The core loss in the sun gear laminations is slightly higher in the configuration with the magnet carrier, but the impact is small compared to the difference in the magnet eddy current loss. The surface mounted configuration achieved a slightly higher stall torque (calculated with 3D FEA). Note that the configuration with the surface mounted magnets is idealized in the sense that no provision is made for a retaining can, which may be required for the outer magnets on the sun gear. This could lead to a drop in the achievable stall torque for the surface mounted configuration. The magnet carrier eliminates the need for any additional retaining cans or magnet fixtures.

Another issue with the surface mounted design in this case was that the manufacturer could not supply magnets thin enough for the design. If thicker magnets are used, the space available for the stator is reduced and the machine's performance is compromised. Although this was an important consideration for the present design, this issue should not present itself in larger machines.

Based on the above considerations, the design employing the magnet carrier was selected for prototyping. In addition to the geometric variables illustrated in Fig. 4, several pole slot combinations were investigated, as reported in [8]. From

TABLE III
OPTIMAL MACHINE DESIGN PARAMETERS

Parameter	Value
Sun gear magnet pitch	0.9 [fraction of pole pitch]
Ring gear magnet pitch	0.9 [fraction of pole pitch]
Inner modulator pitch θ_{mi}	0.5 [fraction of segment pitch]
Outer modulator pitch θ_{mo}	0.47 [fraction of segment pitch]
Stator yoke thickness t_{sty}	6.6 mm
Stator tooth thickness t_{stt}	24.4 mm
Sun gear magnet thickness t_{sm}	4.7 mm
Sun gear ring thickness	0.8 mm
Sun gear rib thickness	0.6 mm
Modulator thickness t_m	5 mm
Modulator bridge thickness	0.5 mm
Ring gear magnet thickness t_{rm}	2.8 mm
Ring gear yoke thickness	2.8 mm
Slot base θ_{stb}	0.45 [fraction of slot pitch]
Slot opening θ_{sto}	0.34 [fraction of slot pitch]
Slot tip γ_{stp}	0.85 [fraction of tooth thickness]
Number of sun gear pole pairs	5
Number of modulator segments	36
Number of ring gear pole pairs	31
Number of slots	12
Gear ratio	7.2

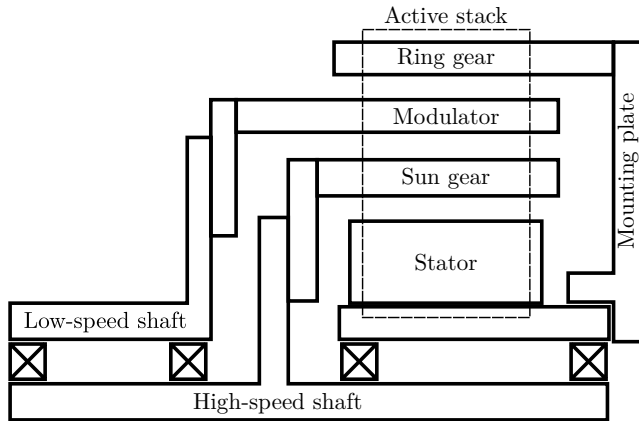


Fig. 5. Mechanical design of the prototype.

these, the best combination was selected. Further attention was then given to be the minimization of cogging torque, which resulted in the final design parameters listed in Table III [8].

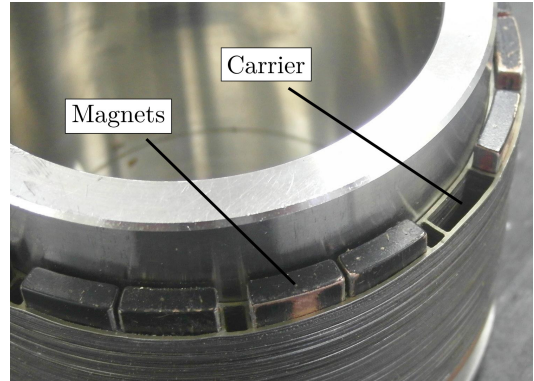
V. PROTOTYPE FABRICATION

The designed MGM consists of four concentric components and as such, its construction is challenging. Fig. 5 gives a rough impression of the mechanical design of the prototype. The design requires four bearings. The sun gear, modulator and ring gear are only supported on one side, which requires the supporting structure, as well as the components themselves, to be stiff.

Some stages of manufacturing process are illustrated in Fig. 6. The stator's non-overlap winding was wound directly onto the teeth – a tedious process. The design could also have been realized with a stator constructed using a separate



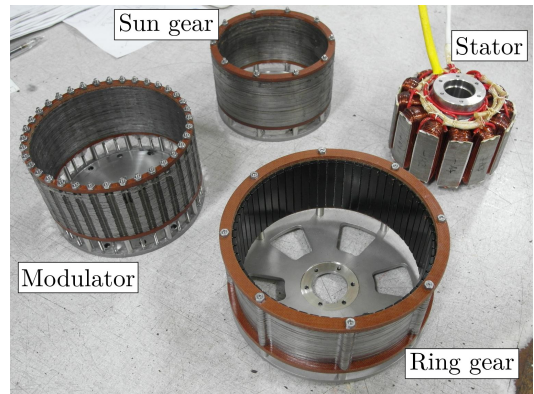
(a) Winding process.



(b) Partially completed sun gear on the mould. Empty mounting channels, magnets and an empty magnet slot are visible.



(c) Modulator support rods. Cavities to be filled with epoxy.



(d) Completed components ready for assembly.

Fig. 6. Fabrication of the prototype.

TABLE IV
WINDING INFORMATION

Parameter	Value
Wire diameter	0.63 mm
Phase resistance R_ϕ	6.3 Ω
Number of turns per coil	212
Fill factor	0.49

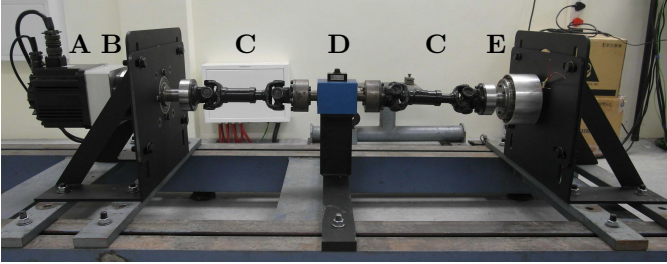


Fig. 7. Setup used to test the prototype. A: servo motor, B: gearbox, C: prop shaft, D: torque sensor, E: MGM prototype

teeth and yoke structure. A winding fill factor of 0.49 was achieved, which is slightly lower than the value used during the optimization. Information related to the winding is given in Table. IV

The sun gear was manufactured using a laminated carrier into which magnets were inserted. This assembly was fixed to a supporting plate by stainless steel rods that were inserted in mounting channels between the magnets. Once the rods were inserted, these channels were filled with resin. The modulator was constructed using a similar approach. Rods connected to a side plate were inserted in the slots between the modulator teeth and the cavity was filled with resin. The ring gear magnets were accurately located by small protrusion on the inner surface of the ring gear yoke and glued in place.

Some problems were experienced in the manufacturing process and the prototype's rotors run with noticeably eccentricity. At certain angular positions, the sun gear makes light contact with the stator. The mechanical design of the prototype and the manufacturing process are areas where significant improvements can be made in future.

VI. PERFORMANCE EVALUATION

Fig. 7 shows the machine on the test bench. A servo motor connected to a gearbox was used to drive the prototype which operated as a generator. The prototype was connected to a resistive load through an autotransformer, which provided a simple method of adjusting the load. A torque sensor measured the input power delivered to the modulator. The generated output power was measured with an oscilloscope as well as two wattmeters.

A. Stall torque test

The gear's stall torque was evaluated by locking the sun gear and rotating the modulator slowly. Fig. 8 shows a waveform of the torque on the modulator during this test. The peak measured torque was 82 Nm (107 kNm/m^3), whilst the simulated

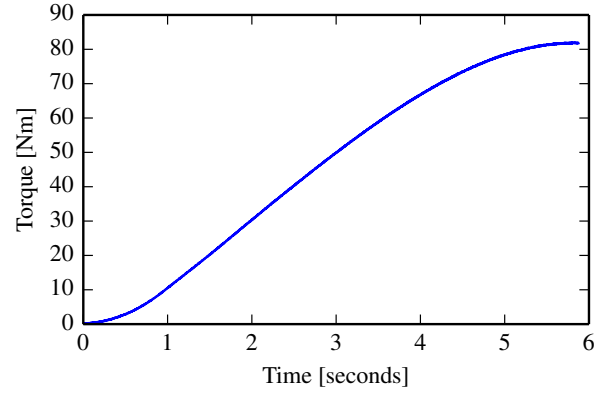


Fig. 8. Measurement of the stall torque.

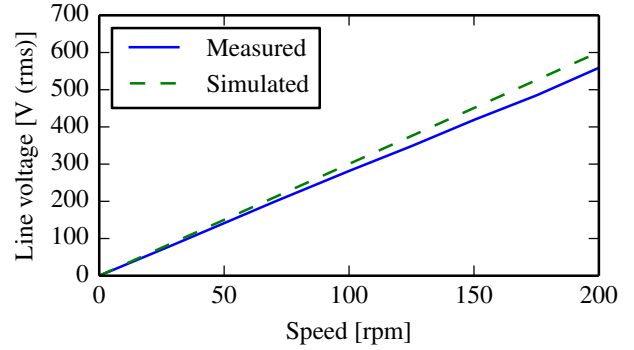


Fig. 9. Measured no-load line voltage versus speed.

stall torque was 88 Nm (115 kNm/m^3). The prototype achieved 93% of its designed stall torque rating.

B. No-load tests

Fig. 9 shows a comparison of the magnitude of the simulated and measured no-load line voltage up to a speed of 200 rpm. The measured voltage is about 7% lower than predicted by the 3D finite element model.

A comparison of the simulated (2D FEA) and measured no-load voltage waveforms at 150 rpm (modulator shaft) is shown in Fig. 10. Besides, the small difference in amplitude, the waveforms are in excellent agreement.

The measured no-load losses are shown in Fig. 11, along with results from transient 2D FEA. The total loss at 150 rpm is almost 100 W, while the losses calculated with transient 2D FEA was only 30 W. The simulated loss does not include losses generated by windage and bearing friction. Although core loss is frequently underestimated by FEA, the high measured loss is largely attributed to factors which are not accounted for in the simulation. As mentioned in section V, the sun gear makes contact with the stator periodically, generating excess friction. Some additional eddy currents can be generated in the stainless steel rods supporting the sun gear and the modulator, even though care was taken to isolate the rods from each other. The rods were not included in the finite element model. Flux leaking to the supporting structure can also cause eddy current losses, but the design was made to limit this. Non-ferrous materials were used for the supporting

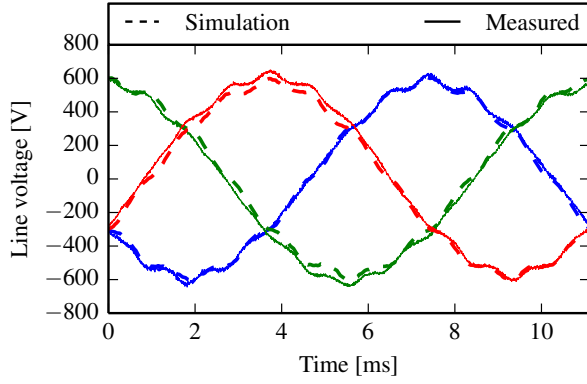


Fig. 10. Comparison of simulated and measured no-load line voltage waveforms.

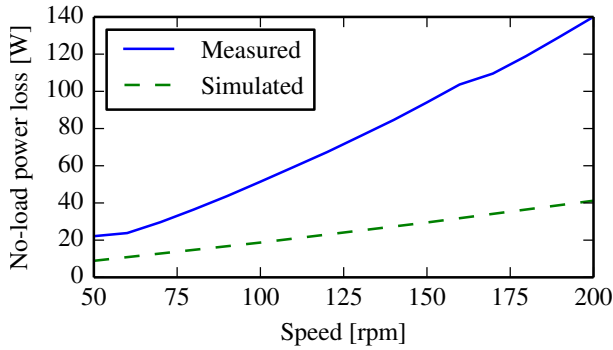


Fig. 11. No load loss curve.

structure and non-conducting spacers were used in areas in close proximity to the active stack. Despite the efforts to limit all these losses, the impact on the performance of the machine is clearly significant. However, these results need not be discouraging, as it is expected that the no-load losses can be greatly reduced through refinements in the design, especially on the mechanical side. Furthermore, the no-load losses were not considered in the optimization process.

C. Load tests

The machine was tested in generator mode over a speed range of 30 – 175 rpm with an input torque ranging between 10 and 60 Nm. The speed was accurately controlled by the driving servo motor. The load on the machine was varied by adjusting the voltage applied to a resistor bank using an autotransformer, which was fed by the machine. An efficiency map of the machine over this operating range is illustrated in Fig. 12. An efficiency above 85% is achieved over a wide operational range. Considering the extra losses incurred due to manufacturing problems, the result is satisfactory. All tests were conducted at a power factor of 0.9 and above.

D. Operating point analysis

In order to verify that the machine's operating points can be simulated accurately, a specific operating point was analyzed in greater depth. Measurements at the considered operating

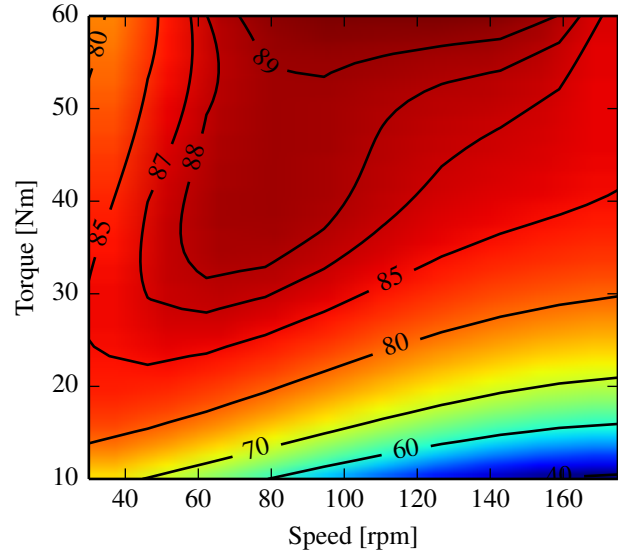


Fig. 12. Efficiency map of the prototype operating in generator mode at a power factor ≥ 0.9 .

TABLE V
COMPARISON OF MEASURED AND PREDICTED OPERATING POINT

	Measured	Predicted	Error [%]
Torque T_m	59.9Nm	65.1 Nm	8.7
Speed n_m	150rpm	150 rpm	0
Line voltage	357 V	374 V	4.8
Phase current	1.43 A	1.50 A	4.9
Input power	940 W	1 023 W	8.8
Output power	835 W	915 W	9.6
Power factor	0.94	0.94	0
Load	$136 + j48 \Omega$	$136 + j48 \Omega$	0
Efficiency	88.9 %	89.4 %	0.6
Load angle δ_g	n.a.	-55.5°	n.a.

point are listed in Table V. The voltage, current and power factor uniquely define the load. The load angle of the magnetic gear δ_g could not be measured. This measurement would require two position sensors, one for the modulator and one for the sun gear.

For conventional machines, an operating point is uniquely defined by three parameters: (ω, i_d, i_q) with ω the angular frequency (speed), and i_d and i_q the dq currents. In magnetically geared machines, these three parameters alone are not sufficient to define a unique operating point. The magnetic gear's load angle δ_g is also required. A procedure for finding an operating point (i_d, i_q, δ_g) given ω and the load impedance, Z_L , can be outlined as follows:

- 1) Map $\lambda_d, \lambda_q, T_s$ and T_m versus i_d, i_q and δ_g , giving

$$\begin{aligned} \lambda_d(i_d, i_q, \delta_g), \quad \lambda_q(i_d, i_q, \delta_g) \\ T_s(i_d, i_q, \delta_g), \quad T_m(i_d, i_q, \delta_g) \end{aligned} \quad (14)$$

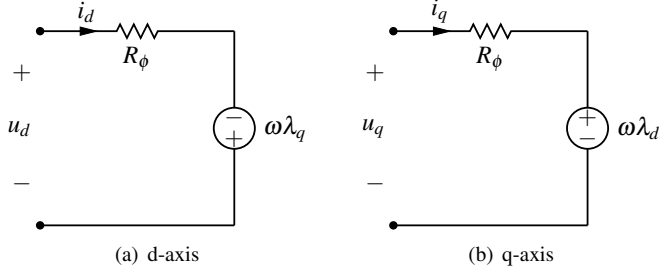


Fig. 13. Equivalent circuit models.

2) Find i_d , i_q and δ_g such that

$$T_s(i_d, i_q, \delta_g) - \beta \frac{P_{rot}}{\omega_s} = 0 \quad (15)$$

$$-i_d R_L + i_q X_L = -\omega \lambda_q(i_d, i_q, \delta_g) + R_\phi i_d \quad (16)$$

$$-i_d X_L - i_q R_L = \omega \lambda_d(i_d, i_q, \delta_g) + R_\phi i_q \quad (17)$$

Equation 15 enforces the condition that the net torque on the sun gear is zero for steady state operation. The second term in (15) accounts for the rotational losses associated with the sun gear, including core loss, magnet loss and windage and friction loss. The total rotational loss is P_{rot} and β is a parameter between 0 and 1 which determines the distribution of the loss between the sun gear and the modulator. Using this model, the torque on the modulator is calculated as

$$T_m^l = T_m(i_d, i_q, \delta_g) + (1 - \beta) \frac{P_{rot}}{\omega_m} \quad (18)$$

where P_{rot} is calculated as the difference between the total measured loss at the operating point and the known (calculated) copper loss.

Equations 16 and 17 are derived from the dq equivalent circuits for the MGM, shown in Fig. 13 and from the relationship between the load and the machine's terminal voltages and currents:

$$R_L + jX_L = \frac{u_d + ju_q}{-(i_d + ji_q)} \quad (19)$$

In the equivalent circuits of Fig. 13, the flux-linkages λ_d and λ_q represent the total flux linkage, including contributions from the sun gear, the ring gear and end-windings. In this investigation, these flux linkages were calculated using 3D FEA.

When generating the map, it is important that the power balance is maintained accurately. This can be verified by ensuring that (6) is satisfied. When single point simulations are used to construct the mapping, it is better to calculate the torque on the stator and the sun gear using (10) and (11). Using this approach, the average torque can be estimated from a single point even though cogging torque and torque ripple have an influence on the instantaneous torque at the simulated point.

The predicted values in Table V were obtained using the described method. A reasonable level of accuracy is achieved, considering the number of stages at which errors are introduced.

The maps in (14) can be used to obtain various important characteristics of the machine over its operational range. For example, the maximum output power (generator operation) given a voltage and current limit can be found for the machine's operational speed range. This can be achieved by solving the following optimization problem over the required speed range:

$$\text{Maximize: } P(i_d, i_q, \delta_g) = \frac{3}{2}(i_d u_d + i_q u_q) \quad (20)$$

$$u_d = -\omega \lambda_q(i_d, i_q, \delta_g) + R_\phi i_d \quad (21)$$

$$u_q = \omega \lambda_d(i_d, i_q, \delta_g) + R_\phi i_q \quad (22)$$

$$\text{Subject to: } T_s(i_d, i_q, \delta_g) = 0 \quad (23)$$

$$I_\phi = \frac{1}{\sqrt{2}} \sqrt{i_d^2 + i_q^2} < I_{max} \quad (24)$$

$$U_\phi = \frac{1}{\sqrt{2}} \sqrt{u_d^2 + u_q^2} < U_{max} \quad (25)$$

In the formulation above, only copper loss is considered, but the method can be generalized to include other loss components. The prototype's maximum operational range mapped in this way is shown in Fig. 14.

VII. CONCLUSION

This paper has reported on the design and evaluation of a prototype magnetically geared machine (MGM) with a novel structure for the sun gear (high-speed rotor). An analysis and optimization methodology has been presented which allows MGMs to be designed by using finite element simulations efficiently.

Although some difficulty was experienced in the manufacturing process, the prototype shows good performance and achieved 93% of its stall torque rating, corresponding to an active volume torque density of 107 kNm/m³.

A method of analyzing the operating points of magnetically geared machines has been presented. The method requires that a map of the dq flux linkages and the torque on the various components versus the dq currents and the magnetic gear's load angle be generated. With such a map available, the operating point (i_d, i_q, δ_g) given a certain load can be found. The method can also be employed to obtain other important machine characteristics such as the maximum torque per ampere curves or the maximum output power given voltage and current limits.

It is expected that a reduction in the no-load losses can be achieved with improvements in the mechanical design of the machine. The calculation of these losses can also be included in the optimization process in future work, leading to further improvements in the design.

This paper supports existing claims of the exceptionally high torque density that can be achieved with magnetically geared machines. These machines have great potential in low-speed, high-torque applications.

APPENDIX LOAD ANGLE DERIVATION

For simplicity's sake, assume that the sun and ring gear magnetomotive forces (MMF), as well as the modulator per-

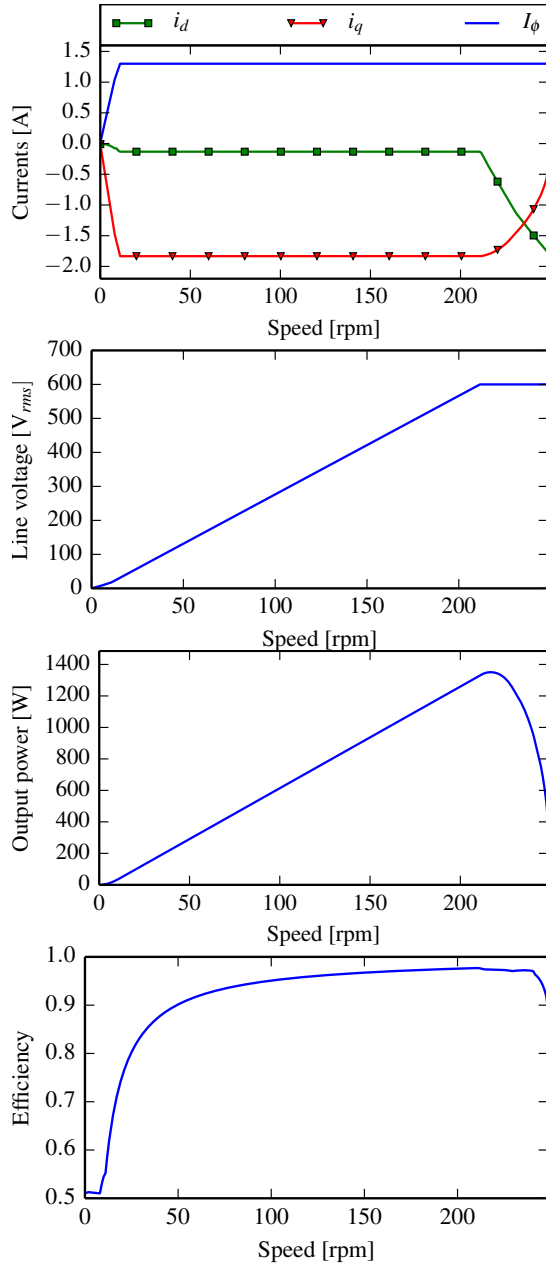


Fig. 14. Maximum output power characteristics with a line voltage limit of 600 V and a phase current limit of 1.3 A.

meance function can be represented by sinusoidal functions of angular position θ :

$$\mathcal{F}_s = M_s \cos(p_s(\theta - \theta_s)) \quad (26)$$

$$\mathcal{F}_r = M_r \cos(p_r(\theta - \theta_r)) \quad (27)$$

$$\mathcal{P}_m = P_m \cos(q_m(\theta - \theta_m)) \quad (28)$$

where M_s , M_r and P_m are magnitudes and θ_s , θ_r and θ_m are the offset angles illustrated in Fig. 2. For the purpose of this derivation, the flux modulation effect is modelled such that, for each MMF source, the interaction of the MMF and the modulator permeance produce a flux distribution containing

three space harmonics:

$$\begin{aligned} \phi_s &= \phi_{sf} + \phi_{s+} + \phi_{s-} \\ &= C_{sf} \cos(p_s(\theta - \theta_s)) + \\ &\quad C_{s+} \cos(p_s(\theta - \theta_s) + q_m(\theta - \theta_m)) + \\ &\quad C_{s-} \cos(p_s(\theta - \theta_s) - q_m(\theta - \theta_m)) \end{aligned} \quad (29)$$

$$\begin{aligned} \phi_r &= \phi_{rf} + \phi_{r+} + \phi_{r-} \\ &= C_{rf} \cos(p_r(\theta - \theta_r)) + \\ &\quad C_{r+} \cos(p_r(\theta - \theta_r) + q_m(\theta - \theta_m)) + \\ &\quad C_{r-} \cos(p_r(\theta - \theta_r) - q_m(\theta - \theta_m)) \end{aligned} \quad (30)$$

with the constants C denoting a specific magnitude throughout this section. In each case, the first term has the same order as that of the source MMF. The second and third terms are due to the interaction of the source MMFs and the modulator's permeance. Two harmonics are generated according to the identity:

$$\cos A \cos B = \frac{1}{2} [\cos(A + B) + \cos(A - B)] \quad (31)$$

In reality, the harmonics' magnitudes vary with radial position, but for this derivation, they can be assumed to be constant without affecting the result. From (29) and (30), it can be seen that if the fundamental harmonics from the sources are to interact usefully with the modulated harmonics (and assuming that $p_s < p_r$), then

$$p_r = q_m \pm p_s \quad (32)$$

When $p_r = q_m + p_s$, the working harmonics are ϕ_{sf} , ϕ_{r-} , ϕ_{rf} and ϕ_{s+} . Otherwise, when $p_r = q_m - p_s$, the working harmonics are ϕ_{sf} , ϕ_{r-} , ϕ_{rf} and ϕ_{s-} . The torque transfer capability is better in the latter case and so, for the remainder of this discussion, it is assumed that $p_r = q_m - p_s$.

The torque on a specific component can be calculated as the derivate of the co-energy in the machine with respect to the angular position of the component. For the modulator,

$$T_m = \frac{\partial W'}{\partial \theta_m} \quad (33)$$

with

$$W' = C_w \int_0^{2\pi} (\phi_s + \phi_r)^2 d\theta \quad (34)$$

Expanding (34) using (29) and (30) results in 36 terms. Of these, only terms with cosines of the same order contribute to the integral

$$\begin{aligned} W' &= C_w \int_0^{2\pi} (\phi_{sf}^2 + \phi_{s+}^2 + \phi_{s-}^2 + \phi_{rf}^2 + \phi_{r+}^2 + \phi_{r-}^2 + \\ &\quad 2\phi_{sf}\phi_{r-} + 2\phi_{rf}\phi_{s-}) d\theta \end{aligned} \quad (35)$$

When taking the derivate of (35), only the last two terms contribute, because all the other terms are independent of θ_m .

Then, the torque is

$$\begin{aligned}
T_m &= C_w \frac{\partial}{\partial \theta_m} \int_0^{2\pi} (\phi_{sf} \phi_{r-} + \phi_{rf} \phi_{s-}) d\theta \\
&= \pi C_w \frac{\partial}{\partial \theta_m} [C_{sf} C_{r-} \cos(-p_s \theta_s - p_r \theta_r + q_m \theta_m) + \\
&\quad C_{rf} C_{s-} \cos(-p_s \theta_s - p_r \theta_r + q_m \theta_m)] \\
&= \pi C_m q_m \sin(p_s \theta_s + p_r \theta_r - q_m \theta_m)
\end{aligned} \tag{36}$$

The argument of the sine function is the load angle. Similar formulae can be derived for the torque on the sun and ring gears, with the same load angle.

ACKNOWLEDGMENT

This work was supported in part by ABB Corporate Research, Sweden, the National Research Foundation (NRF), South Africa and Stellenbosch University.

REFERENCES

- [1] C.-T. Liu, H.-Y. Chung and C.-C. Hwang, "Design assessments of a magnetic-gear double-rotor permanent magnet generator," *IEEE Trans. Magn.*, vol. 50, no. 1, pp. 1–4, Jan 2014.
- [2] K. Chau, D. Zhang, J. Jiang, C. Liu and Y. Zhang, "Design of a magnetic-gear outer-rotor permanent-magnet brushless motor for electric vehicles," *IEEE Trans. Magn.*, vol. 43, no. 6, pp. 2504–2506, 2007.
- [3] P. Rasmussen, T. V. Frandsen, K. K. Jensen and K. Jessen, "Experimental evaluation of a motor integrated permanent magnet gear," in *IEEE Energy Conv. Congress & Expo. (ECCE)*, pp.3982-3989, 2011.
- [4] L. Jian, K. Chau and J. Jiang, "A magnetic-gear outer-rotor permanent-magnet brushless machine for wind power generation," *IEEE Trans. Ind. Appl.*, vol. 45, no. 3, pp. 954–962, 2009.
- [5] K. Atallah, J. Rens, S. Mezani and D. Howe, "A novel "pseudo" direct-drive brushless PM machine," *IEEE Trans. Magn.*, vol. 44, no. 11, pp. 4349–4352, 2008.
- [6] N. Niguchi, K. Hirata, E. Morimoto and Y. Ohno, "Magnetizing directions of the permanent magnets of the magnetic-gear motor," in *IEEE Int. Conf. on Electr. Machines (ICEM)*, Sept 2014, pp. 1279–1285.
- [7] R.-J. Wang, L. Bronn, S. Gerber and P. Tlali, "Design and evaluation of a disc-type magnetically geared PM wind generator," in *Int. Conf. Power Eng., Energy & Electr. Drives (POWERENG)*, pp.1259-1264, 2013.
- [8] S. Gerber and R.-J. Wang, "Design of a magnetically geared PM machine," in *Int. Conf. on Power Eng., Energy & Electr. Drives*, pp.852-857, 2013.
- [9] K. Atallah and D. Howe, "A novel high-performance magnetic gear," *IEEE Trans. Magn.*, vol. 37, no. 4, pp. 2844–2846, 2001.
- [10] C.-C. Huang, M.-C. Tsai, D. Dorrell and B.-J. Lin, "Development of a magnetic planetary gearbox," *IEEE Trans. Magn.*, vol. 44, no. 3, pp. 403–412, 2008.
- [11] F. Jørgensen, T. Andersen and P. Rasmussen, "The cycloid permanent magnetic gear," *IEEE Trans. Ind. Appl.*, vol. 44, no. 6, pp. 1659–1665, 2008.
- [12] K. Davey, L. McDonald and T. Hutson, "Axial flux cycloidal magnetic gears," *Magnetics, IEEE Transactions on*, vol. 50, no. 4, pp. 1–7, April 2014.
- [13] J. Rens, K. Atallah, S. Calverley and D. Howe, "A novel magnetic harmonic gear," *IEEE Trans. Ind. Appl.*, vol. 46, no. 1, pp. 206–212, 2010.
- [14] D. J. Evans and Z. Zhu, "Optimal torque matching of a magnetic gear within a permanent magnet machine," in *IEEE Int. Electric Machines Drives Conference (IEMDC)*, pp.995-1000, 2011.
- [15] S. Gerber and R.-J. Wang, "Analysis of the end-effects in magnetic gears and magnetically geared machines," in *IEEE Int. Conf. on Electr. Machines (ICEM)*, 2014.
- [16] G. Vanderplaats, "A robust feasible directions algorithm for design synthesis," in *24th Structures, Structural Dynamics and Materials Conference*, 1983.